Surface-phonon dispersion curves of KBr(001) via helium-atom scattering: Comparison with calculations

G. Chern and J. G. Skofronick
Department of Physics and Center for Materials Research and Technology, Florida State University, Tallahassee, Florida 32306

W. P. Brug and S. A. Safron
Department of Chemistry and Center for Materials Research and Technology, Florida State University, Tallahassee, Florida 32306

(Received 19 December 1988)

A helium-atom surface-scattering instrument, employing a time-of-flight technique to observe inelastically scattered He atoms, has been used to measure the surface-phonon dispersion curves of the KBr(001) surface. Data were collected in the two high-symmetry directions, ⟨100⟩ and ⟨110⟩, over the entire Brillouin zone for a target temperature of ~115 K and incident He wave vector $k_i \approx 7$ Å^{-1}. The results show important differences from some theoretical predictions of shell-model calculations that use parameters obtained by fitting bulk dispersion curves. In addition, the measured surface dispersion curves of KBr and of RbCl (reported previously) deviate from "mirror-symmetry" behavior, unlike their bulk dispersion curves.

I. INTRODUCTION

The most elementary model for the lattice dynamics of ionic insulators is the rigid-ion model of Kellermann,[1] in which the interactions are basically just the Coulombic attractions and overlap repulsions among the anions and cations. Foldy and co-workers[2] have pointed out that if the Kellermann model provided a complete description of the lattice dynamics of ionic crystals, then reversing the charges of the anions and cations should have no effect on properties of the crystal, which depend on the lattice vibrations. These authors note that for the alkali halides this interchange of charge can almost be "achieved" experimentally. In particular, one should observe "mirror" symmetry in the phonon dispersion curves of pairs of alkali halides such as NaI-CsF, NaBr-RbF, NaCl-KF, and KBr-RbCl, where the masses of the alkali-metal and mirror halide are nearly the same and "extended" symmetry or pseudomonatomic behavior of the phonon dispersion curves in crystals of NaF, KCl, and RbBr, where the masses of the cation and anion are nearly the same. In examing the available data, Foldy and co-workers find that in the latter group the bulk acoustic and optical dispersion curves do nearly match up at the Brillouin-zone edges, and in the first group the dispersion curves of these pairs are indeed similar, especially for the KBr-RbCl pair.

In actually fitting the measured bulk dispersion curves by models of the lattice dynamics,[3] one finds that various shell models which try to account for the polarizability, short-range overlap, and non-nearest-neighbor interactions of the ions give far better agreement with the data than does the Kellermann model. This means that the simple, rigid-ion model is not sufficient to describe the physics of the lattice vibrations. However, one would expect that a close examination of the deviations from extended and mirror symmetry might provide a more probing test of the ability of the shell models to reproduce the true interactions of ions in crystals.

De Wette and co-workers[4–7] have made use of an 11-parameter shell model to calculate the surface dynamics of nearly all of the fcc alkali halides by a slab-dynamics technique. At the same time Benedek and co-workers[8–10] have used the breathing-shell model with a Green's-function technique to calculate the surface dynamics of a number of the same alkali halides, including KBr. Kress *et al.*[7] note, significantly, that "since the bulk [shell models] represent fits to bulk dispersion curves, the models may implicitly contain effects of symmetry cancellations which do not occur at the surface. In other words, surface structure and surface dynamics are more stringent tests for particle-interaction models than bulk structure and bulk dynamics."

The scattering of low-energy He atoms from crystalline surfaces is a nearly ideal way to investigate the static and dynamic properties of insulator surfaces.[9,11–17] The momenta (4–14 Å^{-1}) and energies (10–100 meV) of the He atoms match the momenta and energies of the surface phonons and the atoms do not penetrate, react with, or charge the surface. The intensity of the scattered He atoms as a function of incident angle provides information on the surface geometry, corrugation, and He-surface bound states. The inelastic scattering from single phonon-annihilation or -creation events provides the data from which the surface-phonon dispersion curves can be constructed and, hence, provides information that characterizes the surface dynamics. When these data extend to the Brillouin-zone boundary, the dispersion curves are particularly sensitive to the nature of the forces between surface species.

The first experiments that used atomic beams to determine the surface-phonon dispersion curves of crystals

were carried out on LiF.[11] Since then the only other alkali halides to have been examined by this technique are NaF, NaCl, and KCl, and of these only NaF (which does show extended symmetry behavior) has been studied in detail.[9] In general, these experimental results agree with the slab calculations of de Wette and co-workers[4,7] and with the Green's-function calculations of Benedek *et al.*[8,9] However, Kress *et al.*[7] point out that the surface dispersion curves of the heavier alkali halides, and particularly their optical branches, should be more sensitive to relaxation and to the features of the shell models.

We have recently finished the construction of a new helium-atom surface-scattering instrument for carrying out surface-spectroscopy experiments on a variety of crystalline materials, including the ionic insulators. The alkali halides are the simplest of the latter, which include, for example, the technologically important perovskite crystals $LiNbO_3$ and $BaTiO_3$, among many others. The bulk dynamics measurements of all these crystals have been interpreted with shell models,[3] but there have been no previous He-atom surface-spectroscopic studies on the heavier alkali halide crystals, nor on any of the more complicated ionic insulators. In light of the comments of de Wette and co-workers noted above, we believe that it is important to validate the use of the shell models not just for the calculation of the surface dynamics but also, more fundamentally, for the interpretation of both the surface and the bulk dynamics. Our effort toward understanding the alkali halides is the first step in this direction.

The first results from this new instrument were obtained for the RbCl(001) surface and are reported elsewhere.[18] For this crystal only the lowest-energy S_1 curves (Rayleigh wave) were observed, which agreed fairly well with the slab-dynamics calculations for an unrelaxed surface.[4] In this paper we report the results of measurements on the mirror compound KBr, for which we have been able to observe optical as well as acoustic modes. The general appearance (energies and shapes) of the calculated dispersion curves in these two crystals are somewhat similar. However, the slab calculations for KBr (Ref. 7) predict a crossing surface resonance in each high-symmetry direction that looks like the "sagittal resonance" discussed by de Wette *et al.* for NaCl,[6] which is absent for RbCl.[19] These modes have nearly the same energy as the S_1 modes near the $\bar{X}$ and $\bar{M}$ points in the surface Brillouin zone. We will refer to them here generally as "crossing resonances." The Green's function calculation for KBr (Ref. 10) does not show this feature.

II. EXPERIMENT: HELIUM-ATOM SURFACE SPECTROSCOPY

The apparatus for these experiments is shown schematically in Fig. 1 with a description of some of the components given in Table I. A schematic highlighting the scattering geometry is given in Fig. 2. It is similar in a number of respects to instruments which have been described in the literature.[11,20–23] Briefly, the He beam is produced as a nozzle jet in the source chamber with a ve-

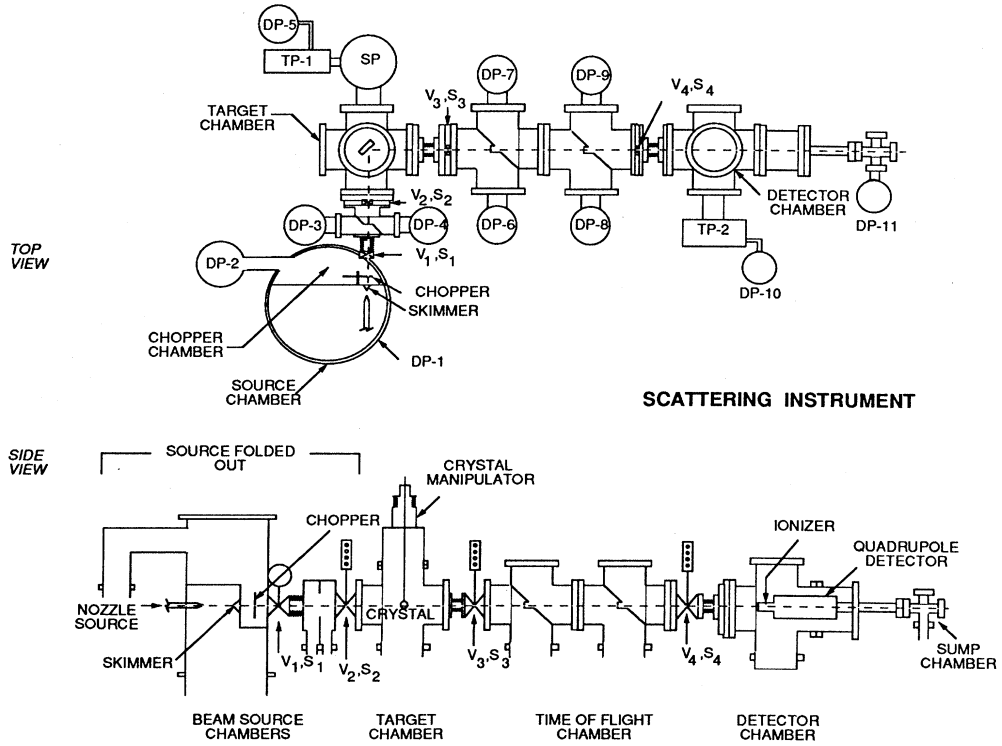

FIG. 1. Schematic of the instrument. The various components are identified in Table I. The sump chamber which follows the detector chamber serves to reduce the background He pressure in the detector region by allowing the considerable fraction of the beam which is not ionized ($>99\%$) to pass through the quadrupole mass spectrometer and be pumped away.

locity spread $\Delta v/v \approx 1\%$.[24] The beam passes through the skimmer into the chopper chamber. For the inelastic-scattering experiments the beam is chopped into pulses which are employed in a time-of-flight (TOF) technique for determining the energy transferred; for the angular distribution experiments the chopper is displaced out of the beam path. In both cases the atoms then pass through two stages of differential pumping to the target chamber, where they collide with the crystal. At the present time the angle between the incoming beam and the detector axis is fixed at 90°.[11] The scattered He atoms then pass through four stages of differential pumping to the detector chamber, where their flux is measured by a quadrupole mass spectrometer operated in a pulse-counting mode.

The nozzle produces a continuous He beam from an aperture with a nominal diameter $d = 30$ μm. Presently it can be operated from room temperature (~ 300 K) down to about 80 K, employing pressures (that vary with the temperature) ranging up to 100 atm. In the experiments reported here the typical operating pressure, $p_0 \approx 35$ atm, produces a He beam with incident wave vector $k_i \approx 7$ Å^{-1}. The $p_0 d$ for these conditions is 80 torr cm, which corresponds to a speed ratio of about 100 and a measured beam full width at half maximum (FWHM) of $\simeq 1.2\%$ (see below). The chopper is normally operated at a frequency of 320 Hz to give pulses with a FWHM of 7 μs. In a TOF experiment the operating pressures in the target and detector chambers are about 5×10^{-10} torr and in the beam path between the crystal and the detector about 2×10^{-9} torr. All the vacuum seals after the security valve V_1 (Fig. 1) are standard ultrahigh-vacuum (UHV) bakable copper gaskets; before the valve the seals are Viton O rings.

TABLE I. Description of apparatus components.

Component	Description
Pumps	
DP-1	Varian HS-20, backed by roots pumps Balzers WKP 1000, WKP 250A and forepump Leybold-Heraeus D-60A
DP-2	Varian VHS-6, backed by forepump Leybold-Heraeus D-30A
DP-3,4,6,7,8,9	Edwards Diffstak 100F, Santovac-5 oil, backed by forepumps Edwards E2M18
DP-5,10	Edwards Diffstak 63C, Santovac-5 oil, backed by forepumps Edwards E2M5
DP-11	Edwards Diffstak 63F, Santovac-5 oil, backed by forepump Edwards E2M2
SP	Ti Sublimation Pump, Leybold-Heraeus V150/2
TP-1,2	Turbomolecular pumps, Balzers TPU-510
Valves	
V_1	Pneumatic security valve, VAT Gate Valve No. 08028-FA40
V_2, V_3, V_4	Variable-aperture valves, Kalrez seals
Slits (defining beam)	
S_1	0.5 mm
S_2, S_3, S_4	Variable apertures—1.5, 3.0, 6.0 mm
Skimmer	1.0 mm, nickel, Beam Dynamics, Inc.
Nozzle aperture	30 μm, molybdenum disk 2.0 mm diam, 0.6 mm thick, Balzers electron-microscope apertures
Manipulator	Wide-bore, Vacuum Generators LBT-165, mounted on differentially pumped rotatable platform, Thermionics RNN-400
Mass spectrometer	Quadrupole, Extrel No. 4-270-9 with power supply No. 011-10 and ionizer No. 041-1, and Galileo No. 4830 Channeltron

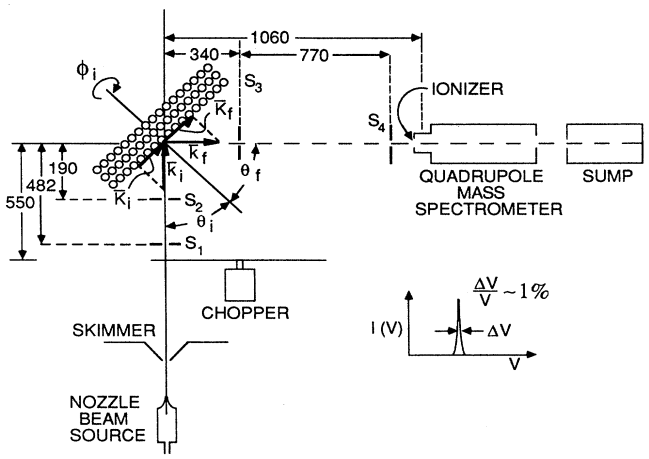

FIG. 2. Schematic showing the geometry of the instrument about the target. The various components are identified in Table I. Distances are given in mm. The angles and wave vectors are defined in the text.

The path length from the chopper to the crystal is 550 mm and that from the crystal to the ionizer of the mass spectrometer is 1060 mm (Fig. 2). The ionizer region is estimated to be, at most, 10 mm long, and, therefore, for a typical He beam used in these experiments, with speeds of about 1100 m/s, contributes a width in the TOF spectra of at most 9 μs. If one assumes that the He velocity distribution, the chopper function, and the ionizer function are approximately Gaussian, then the *measured* TOF width should be the square root of the sum of the squares of the contributing widths. Since the measured width is about 18 μs, the intrinsic beam width is approximately $(18^2-7^2-9^2)^{1/2}=14$ μs, or about 1% of the beam velocity. The path lengths have been checked by direct measurement and have an uncertainty of less than 2 mm. The velocity determinations have been verified by measuring the angular positions of the Bragg peaks of LiF, the surface lattice spacings of which are well known[11] (see below for the conditions for Bragg scattering).

The crystal is mounted on a manipulator which allows it to be aligned in the proper orientation (at the intersection of the beam and detector axes) by permitting translation in the x, y, and z directions, azimuthal rotation, and several degrees of tilting. The heating and LN_2-cooling attachments of the manipulator also permit variation of the temperature of the crystal from approximately 110 to 1300 K. In the experiments reported here the KBr crystal was prepared by cleaving in air and then quickly mounted on the manipulator.[25] The vacuum system was then pumped down and baked for about 24 h at 150°, after which the crystal was heated in vacuum for approximately 2 h at about 675 K. After this procedure the alignment and measurements started. Because of the low surface Debye temperature ($\sim$100 K) for KBr, all the experiments reported here were carried out at target temperatures near 115 K. To prevent contamination at these temperatures, the crystal was periodically flashed at 675 K (usually every 24 h). No evidence of contamination, however, was ever observed.

The manipulator itself is mounted on a differentially pumped rotatable platform so that the incident angle of the He beam onto the crystal, θ_i (measured normal to the crystal surface, see Fig. 2), may be changed without disturbing the alignment controls. A stepper motor under computer control is used to drive the platform. The He beam is calculated to have a cross-sectional area of roughly 5 mm^2 at the crystal, and the calculated angular resolution (FWHM) of the detector is approximately 0.15°.

The data-acquisition system consists of a computer-controlled CAMAC interface which interacts directly with the instrument. The heart of this system is a custom-made multichannel scaler (Lawrence Livermore Laboratory) which is used for the time-of-flight measurements.[26] A security system protects the instrument from damage due to power, water, or vacuum failure.

Three different kinds of experiments can be carried out with this instrument.

A. Angular distribution experiments

Angular distribution experiments are performed by measuring the total scattered intensity of the He beam arriving at the detector as a function of the incident angle of the beam. The condition for Bragg (elastic) scattering is[27]

$$\Delta\mathbf{K}\equiv\mathbf{K}_f-\mathbf{K}_i=\mathbf{G}\ , \tag{1}$$

where $\mathbf{K}_i$ and $\mathbf{K}_f$ (see Fig. 2) are the surface projections of the incident and final He-atom wave vectors $\mathbf{k}_i$ and $\mathbf{k}_f$, respectively, and $\mathbf{G}$ is a surface reciprocal-lattice vector. $K_i=k_i\sin\theta_i$ and $K_f=k_f\sin\theta_f=k_i\cos\theta_i$ for elastic scattering and our 90° apparatus geometry. That is, one expects a Bragg scattering peak only at those angles for which the conditions of Eq. (1) are met. Since the speeds (see below) and angles can be measured, this allows one to determine the surface geometry.

In addition to the Bragg scattering, but at about 2–3 orders of magnitude lower in intensity, the angular distribution contains the inelastic scattering spread out over all angles. However, sharp scattering features due to bound state resonances are usually very evident.[27] We defer discussion of these resonances in KBr to a later paper.

B. Time-of-flight experiments

He-scattering time-of-flight experiments are primarily used to determine the energy transferred to or picked up from the surface at different incident laboratory angles. These data are then used to map out the surface-phonon dispersion curves. The kinematic requirements for single-collision phonon-creation and -annihilation events modify Eq. (1) to[27]

$$\Delta\mathbf{K}\equiv\mathbf{K}_f-\mathbf{K}_i=\mathbf{G}+\mathbf{Q}\ , \tag{2}$$

where $\mathbf{Q}$ is the surface projection of the phonon wave vector, and the phonon energy is

$$\hbar\omega=\hbar^2(k_f^2-k_i^2)/2m\ . \tag{3}$$

A negative value for ω means that a phonon has been created in the atom-surface collision, and a positive value means that a phonon has been annihilated. Thus, by using Eqs. (2) and (3) one can convert the inelastic peaks in the TOF to points on the dispersion curve $\omega(\mathbf{Q})$. More convenient for this purpose is to combine these equations into that of a scan curve,[11]

$$\hbar\omega/E_i=[(\Delta K+k_i\sin\theta_i)^2/k_i^2\cos^2\theta_i]-1 \ . \quad (4)$$

At a given angle θ_i and incident energy $E_i=\hbar^2k_i^2/2m$, Eq. (4) gives the possible values of phonon energy and crystal momentum consistent with Eqs. (2) and (3). That is, the peaks in the TOF spectrum at angle θ_i must correspond to intersections of the scan curve with the surface dispersion curves (or possibly with bulk bands) (see Fig. 7).

C. Low-pressure time-of-flight experiments

Low-pressure time-of-flight experiments on the specularly scattered He beam can be carried out to determine bound-state resonances in the He-surface potential. These are similar to "drift TOF" experiments reported elsewhere.[28–30] The technique involves using low He pressure in the nozzle so as to produce a beam with a broad velocity distribution. One then observes "dips" or "bumps" in the TOF spectrum of the specularly scattered beam wherever the speed or really the wave vector $\mathbf{k}_i$ satisfies the resonance condition[27]

$$\varepsilon_j=\hbar^2(k_i^2-|\mathbf{K}_i+\mathbf{G}|^2)/2m \ , \quad (5)$$

where $\varepsilon_j<0$ is a bound state in the He-surface potential. (Note that this relation also applies to the resonances in subsection A.) A discussion of the bound states of He and KBr and other alkali halides will be left to another paper.

III. RESULTS

A. Angular distributions

1. ⟨100⟩ direction

Figure 3 shows the angular distribution for He scattering from KBr(001) in the ⟨100⟩ direction. The FWHM of the specular peak (0,0) is 0.1°, in agreement with that expected from the slit geometry (0.15°). The angular positions of the peaks correspond to the reciprocal-lattice points G_{nn} as indicated by (n,n) values in the figure. For KBr the calculated spacing from Eq. (1) is 1.89 Å^{-1}, in agreement with the direct lattice constant 6.60 Å.[31] An analysis of the Bragg-peak heights with an eikonal treatment[9,32] gives a peak-to-valley height of about 0.3 Å for the corrugation in this direction. This value is about twice that obtained for the same RbCl surface.[18] That KBr is more corrugated than RbCl is not surprising since Rb and Br lie below K and Cl, respectively, in the Periodic Table. One would therefore expect that Br^- and K^+ are the largest and smallest of these ions, respectively, and that Rb^+ and Cl^- are of comparable size. In the lower half of the figure the vertical scale is expanded by a factor of 100 to reveal the inelastic and bound-state resonance structure refered to above.

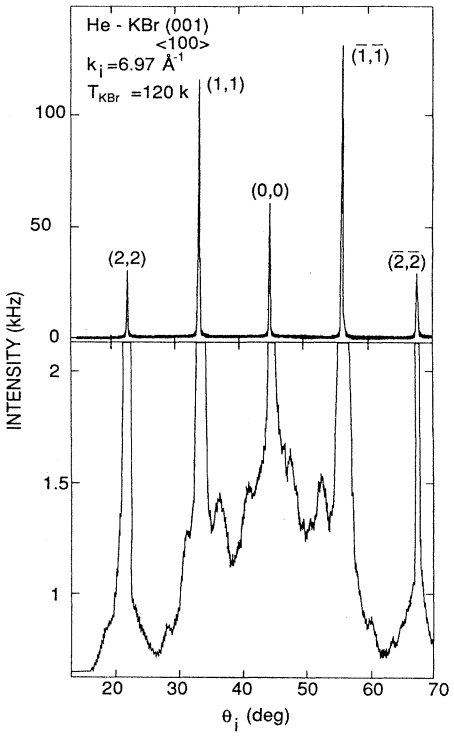

FIG. 3. Angular distribution for the KBr(001) surface in the ⟨100⟩ direction. The lower panel has had the vertical scale expanded by a factor of 100. The intensities are given in kHz.

2. ⟨110⟩ direction

In Fig. 4 we show the angular distribution for KBr(001) in the [110] direction. A comparison with Fig. 3 clearly shows how the differences in both lattice spacing and corrugation show up. In the ⟨110⟩ direction the Bragg peaks correspond to the reciprocal-lattice vectors G_{n0}. From the angular positions in the KBr scan the calculated spacing in reciprocal space in this direction is found to be 1.34 Å^{-1}, in agreement again with the bulk lattice constant given above.

One should note that on the surface the vectors defining the square unit mesh are rotated by 45° from those defining the unit cell in the bulk.[11] ⟨100⟩ is the direction of the KBrKBrKBr. . . rows, whereas ⟨110⟩ is along rows of K's or Br's. On the surface the unit mesh therefore has the length $2\pi/1.34$ Å^{-1}=4.67 Å=6.60 Å/$\sqrt{2}$.

In the lower panel of the figure the vertical scale is again expanded by a factor of 100 to show the inelastic and resonance structure in the angular distribution.

B. Time-of-flight measurements

In Figs. 5 and 6 are shown, respectively, representative series of TOF spectra for KBr in each high-symmetry

direction to illustrate the quality of the data. In comparison with the RbCl spectra which have been reported,[18] one can see that the signal-to-noise ratio is much improved and many more peaks are resolved. The significant difference here is that the operating conditions of the mass-spectrometer ionizer were optimized only after the RbCl crystal had been taken out and replaced. Nevertheless, despite the poorer resolution in the earlier TOF spectra, one can see that there are qualitative differences between the crystals. The richness of these spectra is perhaps illustrated more clearly in Fig. 7, which shows the scan curves, Eq. (4), in the ⟨100⟩ direction for several angles intersecting a number of branches of the surface dispersion curve (adapted from Kress *et al.*[7]). At virtually every one of these intersections, we observe the corresponding peak in the TOF spectrum. Because of the profusion of peaks, our mode assignments are based largely on comparison with the calculations. It is instructive, in fact, to compare the peaks in the spectra

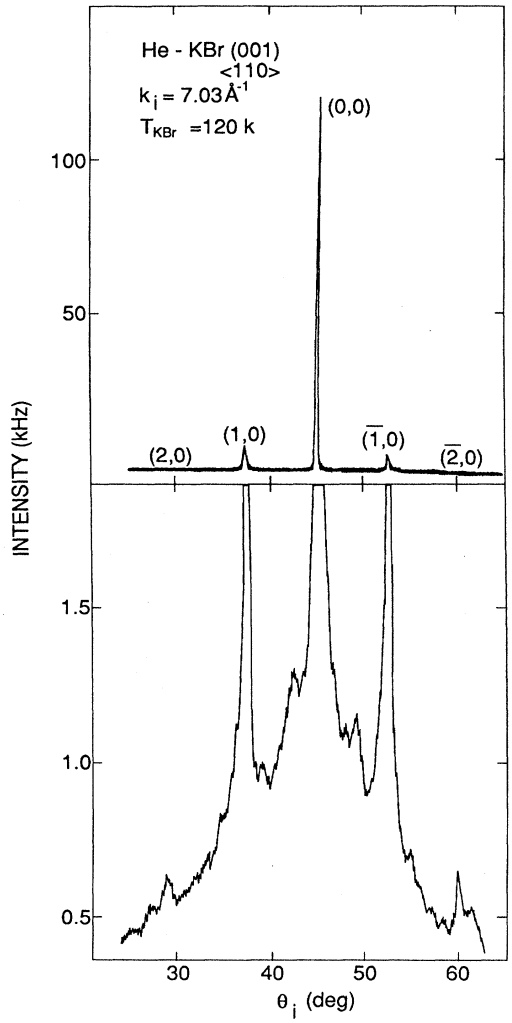

FIG. 4. Angular distribution for the KBr(001) surface in the ⟨110⟩ direction. The lower panel has had the vertical scale expanded by a factor of 100. The intensities are given in kHz.

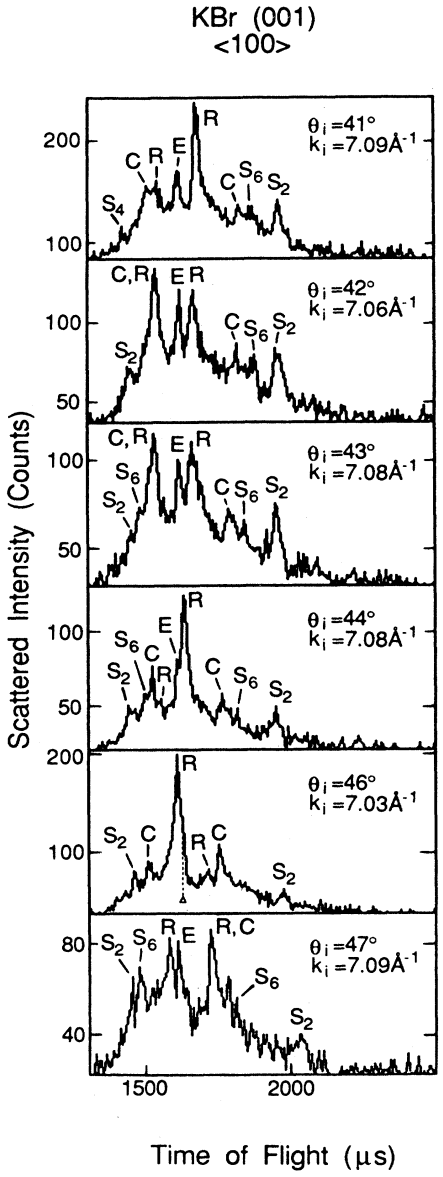

FIG. 5. Representative TOF spectra at several incident angles in the ⟨100⟩ direction. The peaks are labeled following the scheme of Ref. 7, except that the lowest-energy mode S_1 is labeled *R* and the crossing resonance is labeled *C*. Where diffuse elastic peaks are seen, they are labeled with *E*; otherwise the position of the elastically scattered He is shown with a △ and a dashed vertical line. Peaks to the *left* of the elastic position are due to He atoms arriving before the elastically scattered He atoms (greater speed) and therefore correspond to phonon-*annihilation* events; peaks to the *right* are at longer times than the elastic and correspond to phonon-*creation* events. The experiments were carried out such that each channel in the TOF module had a dwell time of 1 μs. The data are displayed as the average number of counts for each consecutive group of six channels; that is, each point shown represents a 6-μs time period. The counting times for these spectra ranged from 2 to 4 h.

shown in Fig. 5 with their corresponding scan curves in Fig. 7. For example, the annihilation peaks in the spectra at 42° and 43° labeled C,R correspond in the scan curves to where the crossing resonance meets the Rayleigh branch at the zone edge ($\overline{M}$). Similarly, one can see that at 46° and 47° the creation peaks labeled S_2 are significantly broadened ($\sim 50-60$ μs FWHM as compared with $\sim 30-40$ μs for other TOF peaks) because, as one sees in Fig. 7, their scan curves intersect the S_2 curve where the slopes are similar; namely, the intersection occurs over a range of phonons. One can see also that the intensities of the peaks for each mode change drastically from angle to angle. In contrast, for the RbCl surface the optical modes had very low intensities when they were observed. Thus, it is clear that the coupling of the He to the lattice vibrations, especially to the relatively higher-energy phonons, is much stronger in KBr than in RbCl.

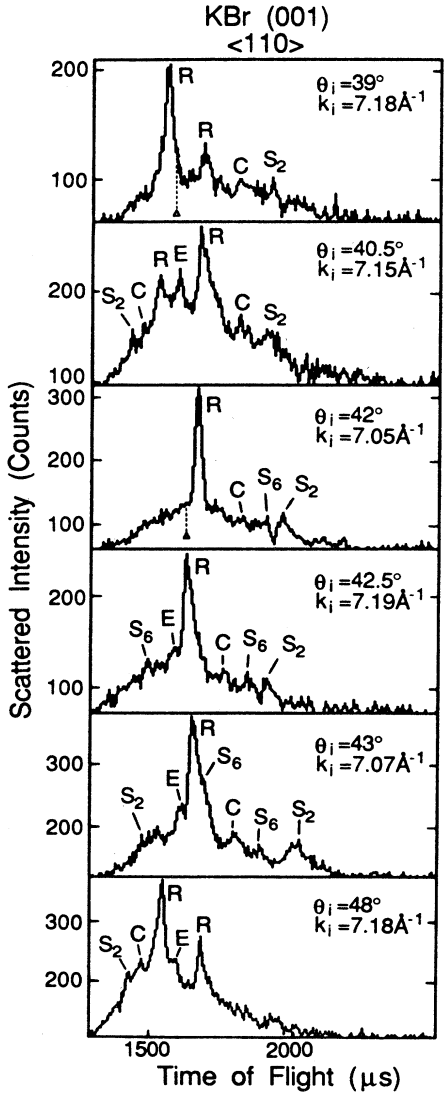

FIG. 6. Representative TOF spectra at several incident angles in the ⟨110⟩ direction. The spectra are shown as in Fig. 5.

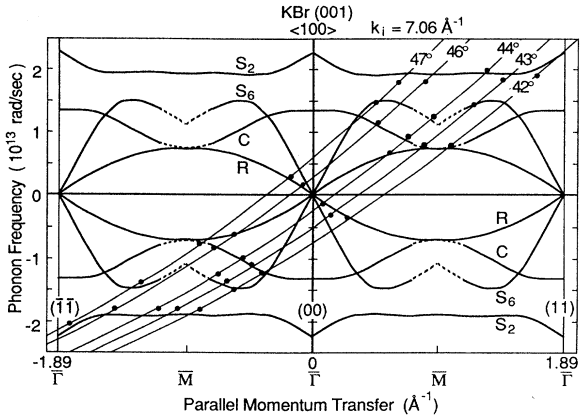

FIG. 7. Scan curves (thin lines) calculated for several incident angles from Eq. (4). The peaks in the TOF spectra lie at the intersections of the scan curves with the dispersion curves (heavy lines and dashed curves) which are adapted from Ref. 7. The labeling of the dispersion curves is as described in Fig. 5. Note that all the scan curves here have been calculated for $k_i = 7.06$ Å^{-1}, although the corresponding TOF spectra in Fig. 5 may have slightly different values. As indicated by Eq. (3), a positive value for ω corresponds to an annihilation event while a negative one corresponds to a creation event.

A second noteworthy feature of the KBr spectra is that the sharp peaks in each TOF spectrum seem to lie on top of a broad "hump" which rises above the noise baseline. In the spectra where the S_2 modes appear, the broad hump seems to drop off sharply before the positions of these peaks. Now, in KBr there is a large gap between the acoustic and optical bulk bands due to the nearly 2:1 mass ratio of the ions. Thus, one might interpret the shape of the TOF spectra as arising from energy transfer to and from the acoustic bulk bands, which gives the broad hump, with the sharp peaks coming in the high-density-of-states region around the surface-localized modes. The abrupt dropoff in intensity, then, reveals the large band gap. There should, of course, be some multiphonon scattering, as well, which also contributes to the hump, but which, at the same time, should tend to obscure the band edge. Modeling calculations to reproduce the TOF spectra are clearly needed to extract the wealth of information contained in the data.

We have calculated the values of $\omega(\mathbf{Q})$ from almost 40 TOF spectra, using Eq. (4). The measured points from the ⟨100⟩ direction are shown in Fig. 8 on top of the dispersion curves in the $\overline{\Gamma}\,\overline{M}$ direction, calculated by de Wette and co-workers,[7] and in Fig. 9 analogously placed on top of the calculations by Benedek and Miglio.[10] Similarly, the values of $\omega(\mathbf{Q})$ in the ⟨110⟩ direction are plotted in Figs. 8 and 9, as above, along the $\overline{\Gamma}\,\overline{X}$ direction. There is obviously a serious disagreement in Fig. 9 because the theoretical predictions do not show the crossing resonance. In both figures our data for the S_1 modes seem to lie somewhat above the calculated values. For the S_2 modes our data seem to lie somewhat below the calculations, except for a "bump" that appears towards the middle of the $\overline{\Gamma}\,\overline{M}$ part of the Brillouin zone. Both of

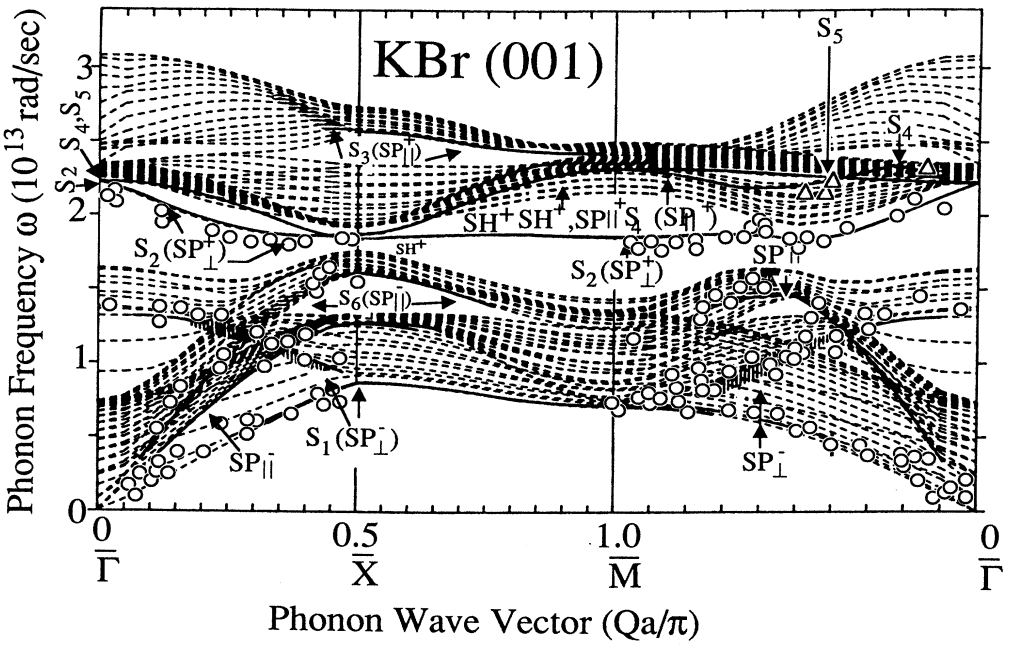

FIG. 8. Surface-phonon dispersion curves for KBr(001) over the entire surface Brillouin zone. The measured values are indicated by open circles, except for open triangles for those points with relatively weaker intensities. Representative error bars are shown in Fig. 9. The slab calculations are taken from Ref. 7.

the calculations have a very slight rise in this same region, but do not match height or sharpness of the measurements. The data along the longitudinal resonance S_6, like those along S_1, seem to lie somewhat higher than the calculations.

IV. DISCUSSION AND CONCLUSIONS

Together with RbCl, the results presented here characterize the lowest-frequency surface-vibrational modes measured to date. In contrast to LiF, which has surface-phonon energies for the S_1 branch at the Brillouin-zone edge of about 22 meV, the corresponding modes of KBr are only about 4.5 meV. However, by using low-energy He beams ($k_i \approx 7$ Å^{-1}) we have been able to measure the dispersion of a number of surface-localized modes for both high-symmetry directions over the entire surface Brillouin zone. Unlike the experiments previously reported for the alkali halides mentioned earlier [except for LiF (Ref. 11)], we find some deviations from the theoretical predictions which are summarized below. This result was, perhaps, anticipated by Kress *et al.*, who stated that the heavier alkali halides would be more sensitive to the features of the shell models.[7]

First and probably the most obvious is that the Green's-function calculation of Kbr by Benedek and Miglio, using the breathing-shell model,[10] does not give the crossing resonances which are shown clearly in the data and also appear in the calculations of Kress *et al.*[7] It is too bad that there are no comparable Green's-function calculations for RbCl; the slab calculations of Chen *et al.*[4] do not show a corresponding crossing resonance here, in agreement with the data.[19] The observation, however, of these resonances in KBr shows that the mechanism proposed by de Wette *et al.*[6] for the similar dynamical behavior in NaCl is probably the correct one and that they are not due to the geometric folding mechanism of Benedek and Miglio.[10]

Second, qualitatively the calculations give the proper shape of the surface-localized modes and resonances, but quantitatively for KBr there are differences as noted

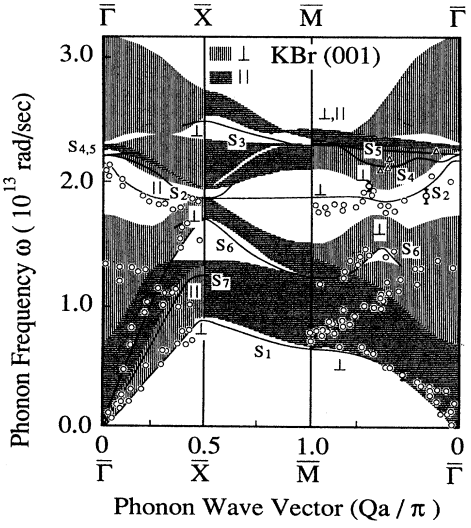

FIG. 9. Surface-phonon dispersion curves for KBr(001) over the entire surface Brillouin zone. The measured values are indicated as described in Fig. 8. Estimated experimental uncertainties are shown as error bars on several points across the Brillouin zone. The Green's-function calculations are taken from Ref. 10.

above. The most noteworthy of these is the sharp bump in the S_2 mode which is different from the very slight rise that comes out of both calculations. The significance for the shell-model description of this feature is not obvious. It may simply be related to the bending of the optical and acoustic band edges in this region of the Brillouin zone. For RbCl the agreement between the data, essentially just the S_1 branch, and the slab calculation[4] is much better, although the data are not as good. But, one does not know whether it is significant that the calculation for RbCl in Ref. 4 neglects surface relaxation, while that for KBr in Ref. 7 includes the relaxation. Perhaps, one should note here that the Green's-function calculation[10] also does not include surface relaxation.

Third, the calculations[7] which give the crossing resonances for KBr suggest that the phonon TOF's in this region should be relatively broad. The TOF data for these peaks, however, are of comparable widths to the peaks for any other surface-localized modes that are observed (except for the S_2 modes noted above). It is interesting that we also find sharp peaks for the crossing resonances of RbBr,[33] where the slab calculations that include relaxation effects[7] also predict broad resonances. In the RbBr case slab calculations are available for the unrelaxed crystal, which seem to agree better with the data. Perhaps the shell-model treatment of the relaxation needs to be explored further.

Finally, the mirror symmetry predicted by Foldy *et al.*[2] for the KBr and RbCl crystals does not seem to carry over to the interaction of the surface with the He-atom probe. The experimental data and the slab-dynamics calculations show that there is a crossing resonance for KBr. Whether a similar resonance exists for RbCl only leads to additional questions: if it exists, why does it not show up in the He-scattering experiments; if it does not exist, what feature of the shell model leads to a difference in the "sagittal resonance mechanism?" Similarly, while the calculations show that both crystals have S_2 modes very similar in energy, the He-atom interaction is very much stronger with the KBr phonons than with the RbCl phonons. For these optical modes the ion doing most of the vibrating is the lighter one, Cl^- in RbCl and K^+ in KBr. Although these ions are isoelectronic, their polarizabilities ought to be quite different, which might account for the different interactions with the scattered He. However, the polarizabilities of these ions obtained from the parameters of the shell model that are used in the surface-dynamics calculations[5] show only a very small difference between them. Perhaps, one needs to examine in detail *all* the factors of the differential reflection coefficient[15] in trying to account for the differences in the interaction of the He with these surfaces.

ACKNOWLEDGMENTS

We acknowledge support from the U.S. Department of Energy under Grant No. DE-FG05-85ER45208. We also wish to acknowledge fruitful discussions with Professor J. P. Toennies, Dr. E. Hulpke, Dr. C. Heimlich, Dr. Ch. Woell, and D.-M. Smilgies of the Max-Planck-Institut für Strömungforschung (Göttingen, Federal Republic of Germany); Dr. R. B. Doak of AT&T Bell Laboratories, Murray Hill, NJ; Professor J. R. Manson of Clemson University, South Carolina; and Professor M. E. Derrick of Valdosta State University, Georgia. We are also appreciative of the assistance we have received from M. Reeves, J. Griffith, C. Keaton, J. Davis, F. Force, and S. Seat. Finally, we wish to acknowledge the considerable efforts of B. Engle, J. Bussey, J. Valentine, M. Cox, and D. Fontaine in the design and construction of the scattering instrument.

[1]E. W. Kellermann, Philos. Trans. R. Soc., London, Ser. A **238**, 513 (1940).

[2]L. L. Foldy and T. A. Whitten Jr., Solid State Commun. **37**, 709 (1981); L. L. Foldy and B. Segall, Phys. Rev. B **29**, 2293 (1984); L. L. Foldy and B. Segall, *ibid.* **25**, 1260 (1982).

[3]H. Bilz and W. Kress, in *Phonon Dispersion Relations in Insulators* (Springer, New York, 1979).

[4]T. S. Chen, F. W. de Wette, and G. P. Alldredge, Phys. Rev. B **15**, 1167 (1977).

[5]F. W. de Wette, W. Kress, and U. Schroeder, Phys. Rev. B **32**, 4143 (1985).

[6]F. W. de Wette, W. Kress, and U. Schroeder, Phys. Rev. B **33**, 2835 (1986).

[7]W. Kress, F. W. de Wette, A. D. Kulkarni, and U. Schroeder, Phys. Rev. B **35**, 5783 (1987).

[8]G. Benedek, Surf. Sci. **61**, 603 (1976).

[9]G. Benedek, G. Brusdeylins, L. Miglio, R. Rechsteiner, J. G. Skofronick, and J. P. Toennies, Phys. Rev. B **28**, 2104 (1983).

[10]G. Benedek and L. Miglio, in *Ab Initio Calculations of Phonon Spectra,* edited by J. Devreese, V. E. van Doren, and P. E. van Camp (Plenum, New York, 1982).

[11]G. Brusdeylins, R. B. Doak, and J. P. Toennies, Phys. Rev. B **27**, 3662 (1983).

[12]J. P. Toennies, in *Surface Phonons,* edited by W. Kress (Springer-Verlag, Berlin, in press), Chap. 5.

[13]T. Engle and K. H. Rieder, *Structural Studies of Surfaces,* Vol. 91 of *Springer Series in Solid-State Sciences,* edited by G. Höhler (Springer-Verlag, Berlin, 1982), pp. 55–90.

[14]H. Hoinkes, Rev. Mod. Phys. **52**, 933 (1980).

[15]J. P. Toennies, in *Dynamics of Gas Surface Interactions,* edited by G. Benedek and U. Valbusa (Springer-Verlag, Berlin, 1982), pp. 208–226.

[16]K. H. Rieder, in *Dynamical Phenomena at Surfaces, Interfaces and Superlattices,* edited by F. Nizzoli, K. H. Rieder, and R. F. Willis (Springer-Verlag, Berlin, 1985), pp. 2–12.

[17]G. Bracco, R. Tatarek, S. Terreni, and F. Tommasini, Phys. Rev. B **24**, 904 (1986).

[18]G. Chern, W. P. Brug, S. A. Safron, and J. G. Skofronick, J. Vac. Sci. Technol. (to be published).

[19]It is possible that the crossing resonances do exist for RbCl,

but were overlooked in the calculations of Ref. 4; F. W. de Wette (private communication).
[20]G. Lilienkamp and J. P. Toennies, J. Chem. Phys. **78**, 5210 (1983).
[21]R. B. Doak and D. B. Nguyen, J. Electron Spectrosc. Relat. Phenom. **44**, 205 (1987).
[22]K. D. Gibson and S. J. Sibener, J. Chem. Phys. **88**, 7862 (1988).
[23]R. David, K. Kern, P. Zeppenfeld, and G. Comsa, Rev. Sci. Instrum. **57**, 2771 (1986).
[24]J. P. Toennies and K. Winkelmann, J. Chem. Phys. **66**, 3965 (1977).
[25]Crystal Growth Laboratory, Department of Physics, University of Utah, Salt Lake City, UT 84112.
[26]The design is that of P. S. Weiss, Ph.D. thesis, University of California, Berkeley, 1986.
[27]For example, see G. Boato and P. Cantini, in *Advances in Electronics and Electron Physics,* edited by P. W. Hawkes, (Academic, New York, 1983) Vol. 60, pp. 95–160.
[28]G. Drolshagen, A. Kaufhold, and J. P. Toennies, Israel J. Chem. **22**, 283 (1982).
[29]R. B. Doak and D. B. Nguyen, in Proceedings of the Sixteenth International Symposium on Rarefied Gas Dynamics, Pasadena, 1988 (unpublished).
[30]E. Semerad, P. Sequard-Base, and E. M. Hoerl, Surf. Sci. **189**, 975 (1987).
[31]R. W. G. Wyckoff, *Crystal Structures* (Wiley, New York, 1964), Vol. 1.
[32]U. Garibaldi, A. C. Levi, R. Spadacini, and G. E. Tommei, Surf. Sci. **48**, 649 (1975).
[33]G. Chern, W. P. Brug, S. A. Safron, and J. G. Skofronick, Phys. Rev. B (to be published).